VALIDATION OF AN SEA MODEL OF THE OLYMPUS SATELLITE

M G Smith

Institute of Sound and Vibration Research Consultancy Services,
University of Southampton, Southampton, SO17 1BJ. UK.
Tel: +44 (0)1703 592337 Fax: +44 (0)1703 592728

ABSTRACT

As part of studies to predict the high frequency response of the Artemis satellite to mechanical vibration inputs a Statistical Energy Analysis model of the Olympus STM was produced and validated against experimental data obtained in the ESTEC LEAF facility.

The experimental data was processed to give response at many locations around the Olympus STM for a unit power input to the site of a reaction wheel on the service module floor. This type of data is ideally suited to validation of an SEA model since uncertainty in the mobility of the drive point is removed from the model.

The response measured at each test point location on the STM varied widely with the local mass loading of the test point and with the remoteness of the point from the excitation. Given that the precise mass-loading at each test point was not known, the SEA model was able to predict the mean response of each panel of the STM with reasonable accuracy.

The SEA model also used test data obtained in a vacuum chamber at ISVR showing that, except at the critical frequency of the honeycomb panels, the damping of the structure is dominated by damping associated with the built-up nature of the structure, rather than with natural damping of the panels or with other air-damping mechanisms. Some methods and findings of this study are reported here.

The model predicts that vibrational energy flow between the service module floor and the top platform on Olympus is dominated by the path through the central cylinder. The power reaching the top platform is approximately 10% of the power originally injected into the service module floor.

The study was the first opportunity to validate an SEA model using a large database of results, and has enhanced confidence in the predictions of the model.

1. INTRODUCTION

Microvibration on board the Artemis satellite has been identified as potentially a significant problem for the SILEX package. The vibration arises from the operation of mechanisms such as reaction wheels, waveguide switches and thrusters.

Because of size of the structure, and the high frequencies of interest Statistical Energy Analysis was used to predict vibration propagation, [2], but the test data available for validation purposes was always limited.

New test data on damping effects in built up structures and vibration transmission on the Olympus STM provided an opportunity to validate the SEA model, and this is the subject of this paper.

2. DAMPING OF BUILT-UP STRUCTURES IN VACUO

When the damping of a structure is measured, the value obtained includes the effect of all mechanisms by which vibrational energy is removed from the system. In air these mechanisms include:

hysteretic material damping,
friction damping at joints,
damping by sound radiation into the air,
damping by the reactive sound field around the structure,
viscous damping due to air trapped between components.

During previous studies on the high frequency response of the Olympus and Artemis satellites [refs 1 & 2], one of the major uncertainties in the prediction was the level of damping that would be seen on-station in the absence of the three air damping mechanisms. The purpose of the experiment described here, and reported in [3], was to determine the relative importance of the five listed mechanisms on the ground for a structure comprising an assembly of panels and an equipment box. The basic components of the assembly are illustrated in Figure 1. The panels were made of aluminium alloy facing and core, with specification 30 swg 2024T3 x 6mm 3.4 1/4-15P(3003)

Damping tests in air were performed in a small semi-anechoic test chamber (2.0 x 2.6 x 5.0m approx), and in-vacuo tests were performed in a vacuum chamber (900 x 900 x 900mm) belonging to the Department of Cryogenics at Southampton University. A brief trial was performed to find out what working pressure would reduce radiation damping to below the level of material damping. It was found that below 30 mbar there was no change in measured damping. All

Presented at the European Space Agency conference on Spacecraft Structures Materials and Mechanical Testing, March 96, Noordwijk, Netherlands.

subsequent experiments were performed at 20 mbar pressure.

The size of test panels was limited by the need to fit the fully built-up structure into the vacuum chamber and their thickness was chosen in order to give a reasonable modal density compared with typical spacecraft panels. The bending wavelength of honeycomb panels is roughly proportional to the square root of the core thickness. Because the speed of bending waves also has a root frequency dependence, the wavelength at 100 Hz in the 6mm test panel is about the same as the wavelength at 500 Hz in a 30mm thick panel. Besides influencing the critical frequency and radiation damping, it should be noted that there may also be some wavelength dependence of mechanical damping mechanisms which has not been investigated here.

There are four principal methods by which the damping of a structure may be measured, the steady state method, the nyquist plot and half power bandwidth methods, and the time decay method. The first three methods have various restrictions on the class of structure or mode type that can be considered, and this is discussed further in reference [3].

The time decay method is generally applicable to any structure and over any frequency range, and so was the most appropriate method for this study. In this method the structure is excited by a source of vibration. The input is switched off and the rate of decay of the vibration measured. The damping is proportional to this rate of decay.

It is possible to use the time decay method to determine the damping of individual modes of vibration. Either the structure may be excited at a single resonant frequency, or a broad band excitation may be used and the decay of each resonant frequency component obtained by performing two successive Fourier transforms.

The time decay method may also be used to obtain the average damping value for a group of modes within a certain frequency range, and this is the value of damping that is most appropriate for use in an SEA model. It should be noted however that because the damping value may vary considerably from mode to mode within a frequency band, so a time decay may exhibit several slopes. An initial faster than average decay, as highly damped modes are attenuated, is followed by a slower than average decay, as the remaining energy in the plate becomes concentrated in relatively lightly damped modes. For this reason it was necessary to average over a number of excitation points and response points as shown in Figure 1.

The basic experiment is illustrated in Figure 2. The excitation was switched off by making the coil open circuit. This ensured that there was no damping induced in the structure by back-EMF in the driver system.

The B&K 2133 may be programmed to continuously acquire octave band spectra, monitor one of the bands for transition through a trigger level, and perform a least squares fit to the decaying signal. A typical result is shown in Figure 3 for a low, medium and high frequency.

Figure 4 shows measurements of the damping of a bare panel in the two different acoustic environments. When the panel was tested in air there is a strong peak in damping at the coincidence frequency of 2 kHz, with a value twenty times higher than the damping at low frequencies, and five times higher than the damping at high frequencies. It should be noted that the coincidence frequency of typical panels on a satellite such as Olympus is about 300 Hz.

For the plate in-vacuo, the damping can only be due to hysteretic damping of the materials in the composite, i.e. aluminium and adhesive. The loss factors of simple aluminium plates are not strongly frequency dependant, and are typically in the range 0.0005-0.002, depending to some extent on stress levels [ref 4, chapter 25]. Reference 5 shows some typical curves for stiff viscoelastic adhesive at room temperature, showing low damping at low frequencies and a peak at 1-2 kHz. The properties of viscoelastic damping material are temperature dependent, and may provide less damping at the low temperatures sometimes experienced in space.

Figure 4 also shows the effect of attaching an equipment box to an otherwise bare panel. The box causes an increase in damping at all frequencies, and particularly at low frequencies where it is increased by a factor of ten. It is possible that there is some friction damping between the box and the plate, although this seems unlikely to be significant since the base of the box is moulded so that contact only occurs at the feet of the box, and the amplitude of motion in these tests was low. It is more likely that the dominant effect is that the box acts as a damper attached to the plate, with energy being lost through the vibration of internal components of the box. This could be modelled using impedance methods in which the complex impedance of the box (real part from the mass, imaginary part from the damping) is combined with the point impedance of the panel.

Figure 5 compares the damping of the structure comprising all three panels with or without the box attached. It was concluded in the study report [3] that the dominant factor causing the increased damping on the built-up structure at low frequencies, compared with a bare panel of figure 4, was frictional losses at the joints. At this vibration amplitude the frictional losses are a similar order of magnitude to the internal damping of the panels.

Finally it can also be seen by comparing Figures 4 and 5 that the damping measured on the plate and box alone is higher than that measured on the fully built-up structure. In the latter case panel I is heavily

damped by the box, but the decay of energy on panel I is reduced by energy flowing back from the lightly damped panels II and III. It may also be considered that the box (as a damper) will be more effective in damping a single panel than a larger system.

Finally Figure 5 shows the damping on the various builds of structure when the tests are performed in the air. The differences between the full build (i.e. with the box) and the three plates assembly which were observed in-vacuo, are not seen in air. This is to be expected at high frequencies because the differences in total damping around the fully built-up structure are reduced due to the large effect of air damping. This result was not expected at low frequencies but a possible explanation is that the radiation efficiency (and hence radiation damping) of the built-up structure is higher than seen on the bare panel because of the stiffening effect of the joints and the partial baffling which prevents pressure cancelation around some edges of the panels.

3. MEASURED TRANSMISSIBILITY OF THE OLYMPUS STRUCTURE

Reference [6] gives details of tests on the Olympus STM that were performed in the ESTEC LEAF facility by ESTEC staff. The structure was instrumented with seventy-eight accelerometers, suspended in the test chamber, and excited using a swept-sine force input at the location of a reaction wheel and a waveguide switch (with the devices dismounted). At both locations the force input was applied at an angle of 45 degrees to the normal, and thus both flexural and in-plane waves will have been excited.

Figure 6 shows the transfer functions from force input at the reaction wheel location on the service module floor to the test points located on the top platform (communications module floor). The large scatter is due to the highly variable mass or stiffness loading around the platform. Given the scatter in these measurements it is natural to perform a spatial average, and this is shown in Figure 7 for four panels on the STM. The service module floor shows relatively high response at low frequencies but low response at high frequencies. It again appears likely that this is principally due to local mass loading effects at the chosen locations of the test points. The cylinder which is lightly loaded with equipment shows a high response over most of the frequency range.

Figure 8 shows the measured power input per unit force applied to the reaction wheel location, and this is compared with a theoretical prediction of the power input to an infinite panel of the same stiffness and surface density as the Service Module floor. At 450 Hz and above, the infinite panel approximation gives a reasonable estimate of the power input but at lower frequencies the measured power input is more than an order of magnitude lower than predicted. This is because of the stiffening effect of the other STM panels and the cylinder, and mass loading effects of equipment, which reduces the mobility of the service module floor at low frequencies.

The Olympus STM tests also included some tap tests, and these were used to show that the damping of the Olympus structure was broadly in agreement with this data described above except that the lower coincidence frequency of the panels gave a peak in damping in the 250 Hz octave band.

4. SEA MODEL OF OLYMPUS AND COMPARISON WITH THE MEASURED RESULTS

The results described in this section are described in more detail in [7]. The SEA model of the structure was generated using the AutoSEA software [8], and is shown in Figure 9. The model was used to predict the acceleration per unit power input, and this removes the problem of modelling the low frequency power input. In the following comparisons the structural damping loss factor was taken as 0.02, and radiation damping was included in the model explicitly.

As has already been seen, the effect of mass loading is of considerable importance, and the ideal way of handling this is through an impedance model, as described in [9]. In these tests however, the local mass loading at individual accelerometer positions was not known, and so a smeared mass method was applied as the best available option.

Figure 10 shows the prediction and measurement for the top platform, and generally the agreement using smeared mass is quite good. The accuracy of predictions were similar on other panels studied. Across virtually the whole frequency range the predicted mean square acceleration is within a factor of ten of the measurement, i.e. within a factor of three for RMS acceleration.

At low frequencies there are large differences in measured response between adjacent frequency bands due to the low modal density, but the SEA model predicts a good mean value. At high frequencies the smeared mass prediction and the measured curve diverge, and this is because of the approximate mass loading model.

At the location of the PAX accelerometer on the top platform the mass loading effect is known accurately, so it is possible to use the mass impedance method to predict the response. This is shown in Figure 11 and shows excellent agreement with the measurement across most of the frequency range.

The prediction for the cylinder generally under-estimated the measured response, and since not much information concerning the spacing and stiffness of the stiffening rings was available, a more detailed investigation of the structural dynamics of the cylinder would be useful.

Since it appears that knowing the mass loading effect considerably improves the accuracy of the predictions it is clear that ideally the results should be corrected for this before spatial averaging. i.e. either the measured results could have had the mass loading effect taken out so that the comparison should then be with the predicted bare panel response, or the predictions should be made for a number of locations with mass loading incorporated, and then these results averaged for comparison with the spatially averaged test results.

So far we have only considered the vibration response, but the SEA model is also able to predict the flow of vibrational energy around the structure. Figure 12 shows the power losses from the driven service module floor subsystem with a unit power input; radiation damping dominates, and the energy flows fairly equally to all the connected structural components.

Figure 13 shows the net power contributors to vibration on the communications module floor. At all but the highest frequencies the energy from the cylinder is the dominant contributor. Comparing the power flow into and out of the cylinder in Figures 12 and 13 shows that very little energy is dissipated within the cylinder due to the low value of damping on that component.

5. CONCLUSIONS

In order of decreasing importance the damping mechanisms discussed in section 2 were as follows:

- Radiation damping near the coincidence frequency of the test panels. Radiation damping at other frequencies was also significant but not dominant.
- Damping due to an attached box acting as a damper, either through internal friction, friction at the feet or internal material damping.
- Internal damping of honeycomb panels.
- Damping at joints between panels due to friction.

A good understanding of the relative importance of these mechanisms increases confidence in estimates of on-station damping.

The results show that when the loading effects at both the source and receiver points is known, an SEA model is capable of accurate predictions of transfer function. This is shown here by the excellent agreement with the measured response of PAX. It would still be useful to confirm this for a wider range of equipment.

The model predicts that the dominant path for energy flows from the service module floor to the communications platform is through the cylinder.

Figure 13 shows that approximately 0.1 watts/band of power flows into the top platform and this is 10% of the original power input into the service module floor.

6. ACKNOWLEDGEMENTS

The author wishes to thank the European Space Agency (D Eaton, YME (ESA/ESTEC), Noordwijk) for its support of this work. Also thanks to Peter Clarke of ISVR for performing the damping experiments, and to Stuart Dyne of ISVR and staff of the ESTEC LEAF facility for the acquisition and analysis of the Olympus STM results.

7. REFERENCES

[1] Smith, M.G., Prediction of On-Station Vibration on Olympus Measured by PAX, and Assessment of Prediction Model. ISVR-CS Report R10 3930/B7, ESA Contract 9360/91/NL/DG, February 1992.

[2] Smith, M.G., Prediction of Artemis Vibration Environment. ISVR-CS Report R01A 3925/B7, submitted to Alenia Spazio, July 1992.

[3] Smith, M.G., Damping of Built-up Structures In Air and In-Vacuo. ISVR-CS Report R04 4514, ESTEC Contract 7501/87/NL/PP(SC), July 1994.

[4] White and Walker, Noise and Vibration. Ellis Horwood, 1982.

[5] Nashif, Jones, and Henderson, Vibration Damping. Wiley, 1985.

[6] Dyne, S.J.C., Notes on a Mission to ESTEC, 21 and 22 July 1994. ESA P/O 142354, WP 2 Task 1.

[7] Smith, M.G., Transmissibility of Olympus STM. ISVR-CS Report R02 4702. ESA P/O 142354, WP 2.

[8] AutoSEA Software, produce by Vibro-Acoustic Sciences Ltd, Australia.

[9] Structural Acoustics Design Manual, ESA PSS-03-1201, 1995 revision

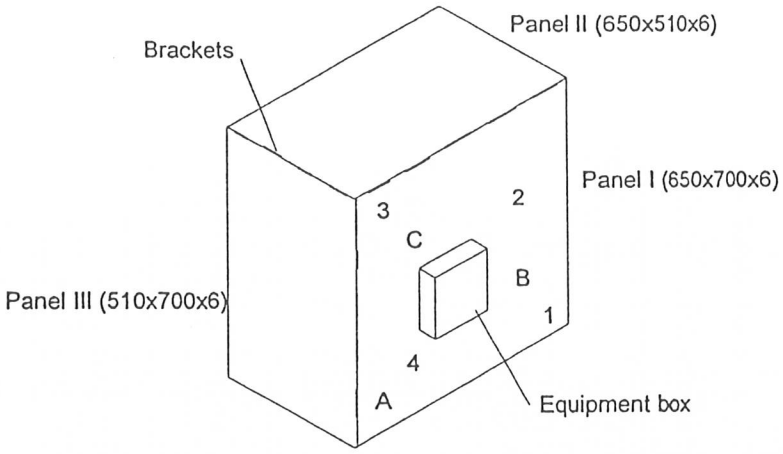

A,B,C = excitation points

1,2,3,4 = response points

total mass of panels and brackets = 3.5kg

mass of box = 1.62 kg

Figure 1. General layout of built-up structure

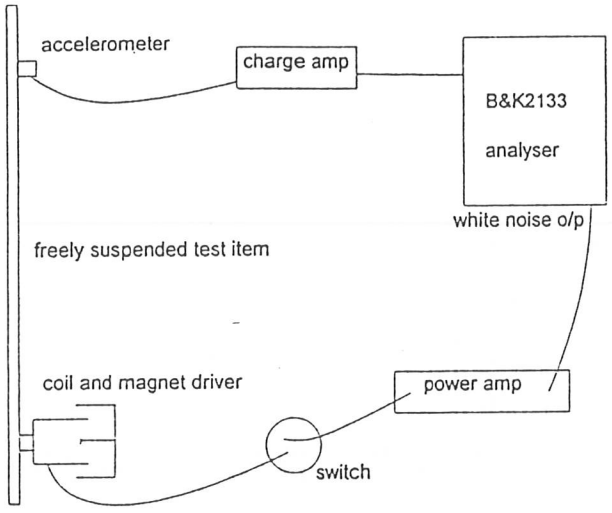

Figure 2. Test set-up for damping measurements

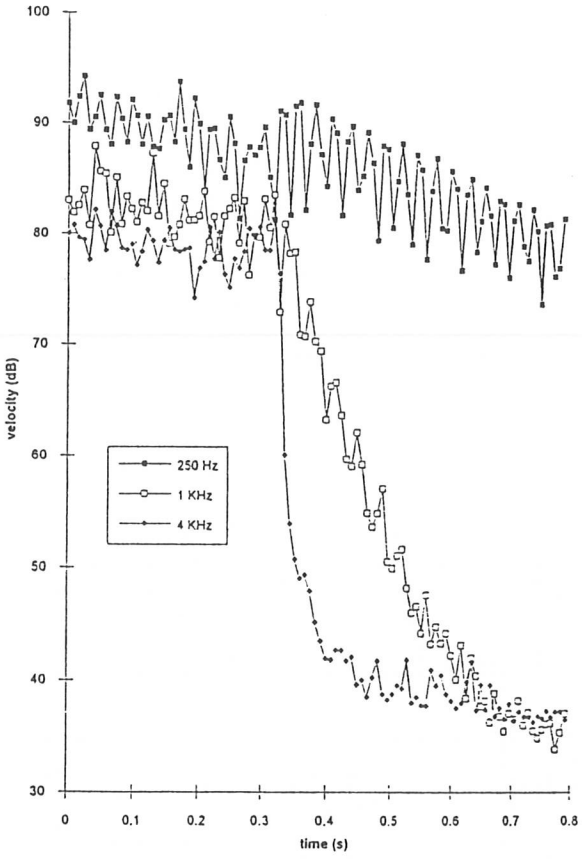

Figure 3. Typical octave band time decays

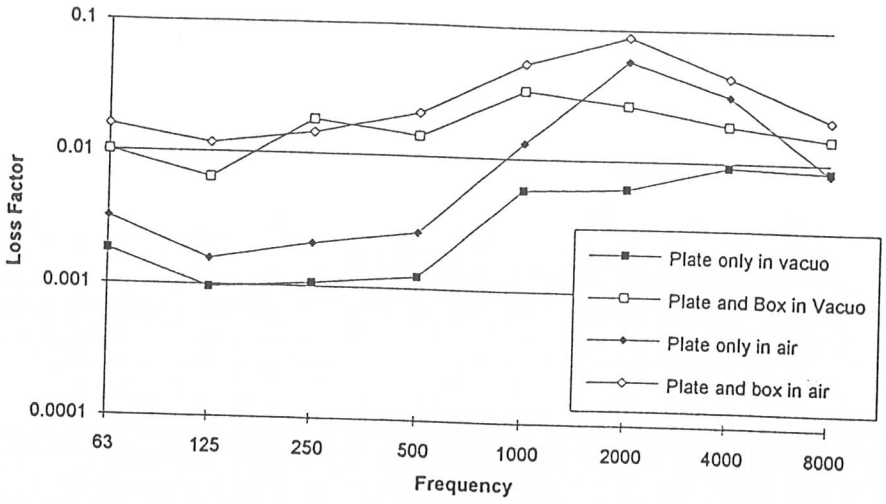

Figure 4. Comparison of in-air and in-vacuo damping on a plate and without a box

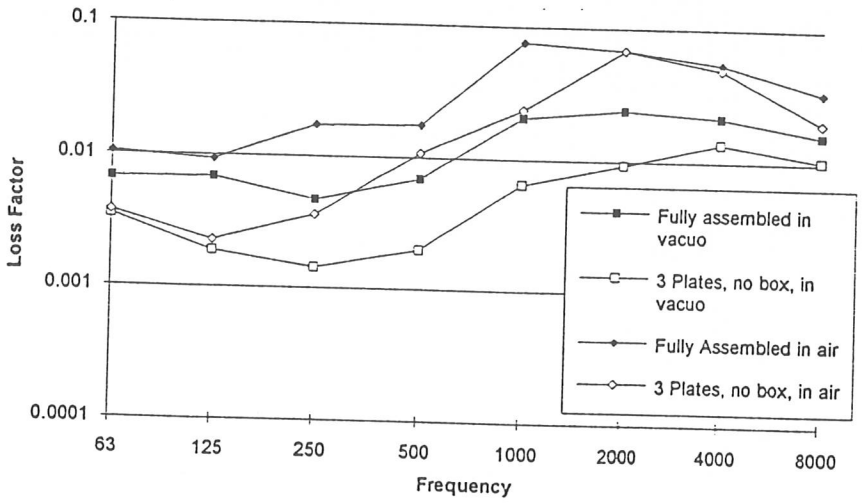

Figure 5. Comparison of in-air and in-vacuo damping on built-up structures

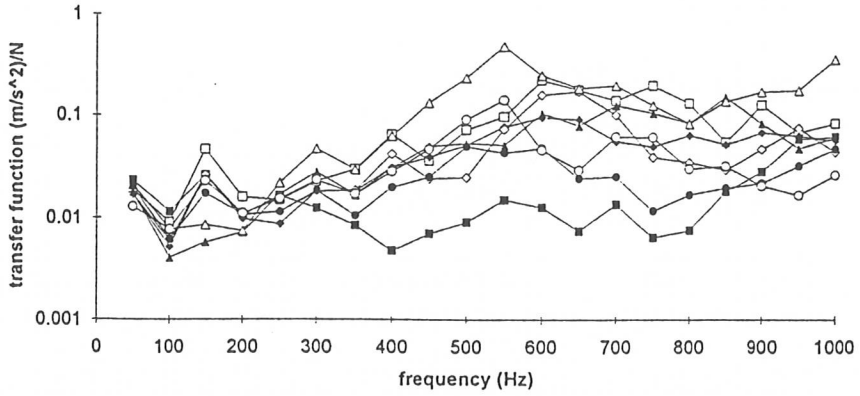

Figure 6. Spatial variation of response on the top platform for a unit force on the SM floor

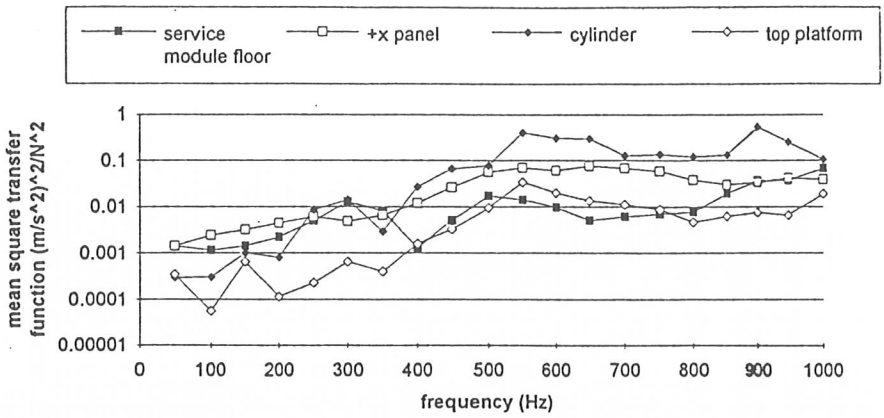

Figure 7. Mean square panel response per unit force on the SM floor

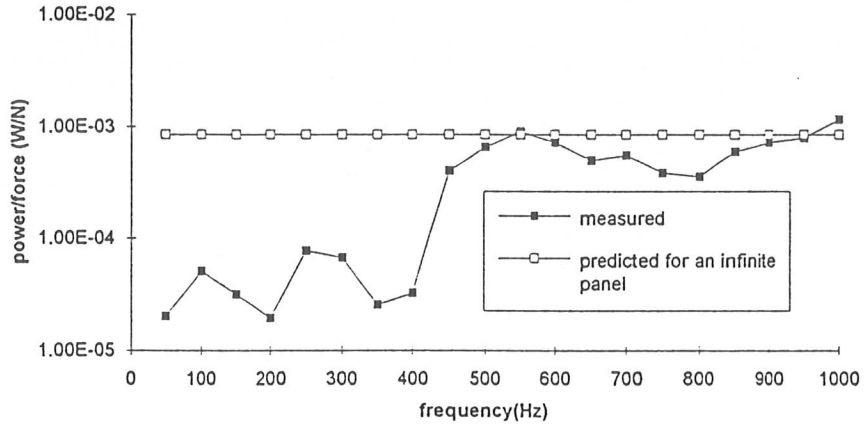

Figure 8. Power input per unit force at SM floor reaction wheel

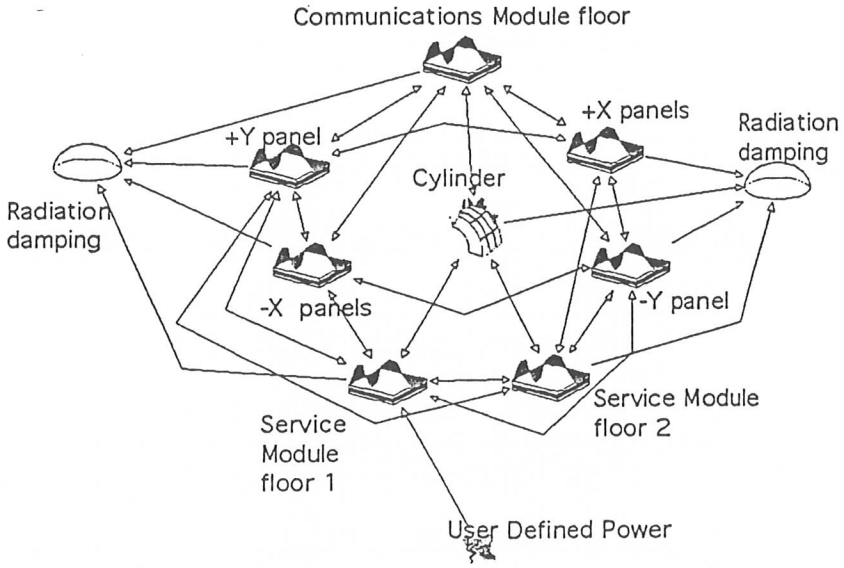

Figure 9. AutoSEA model of Olympus with radiation damping

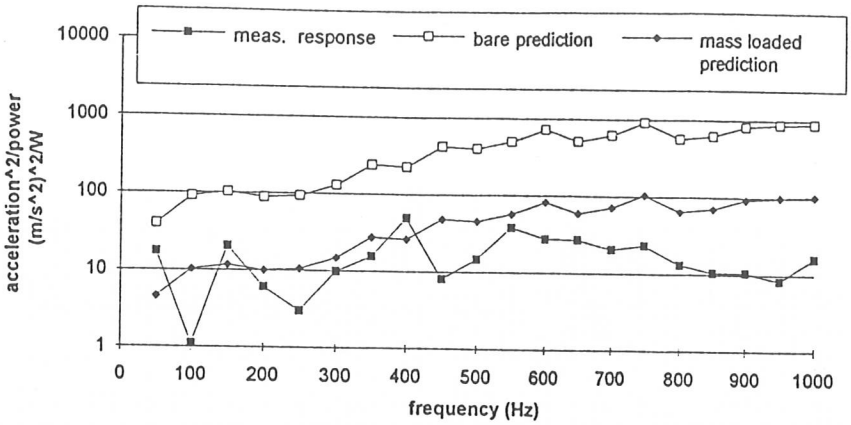

Figure 10. Acceleration response of top platform for unit power into the SM floor

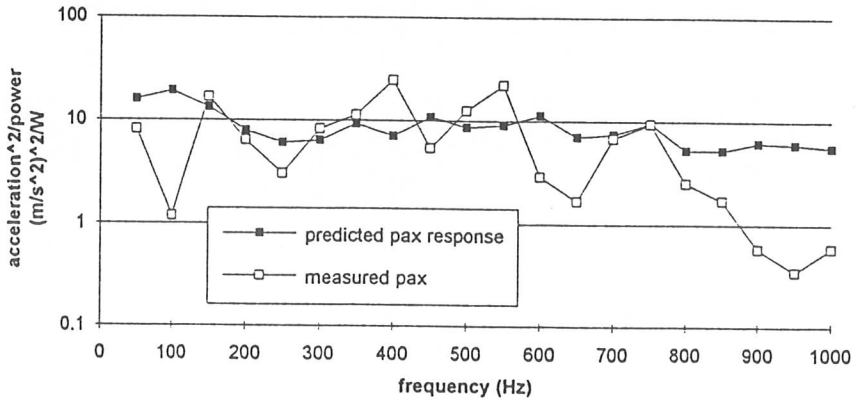

Figure 11. Acceleration response at PAX for unit power into the SM floor

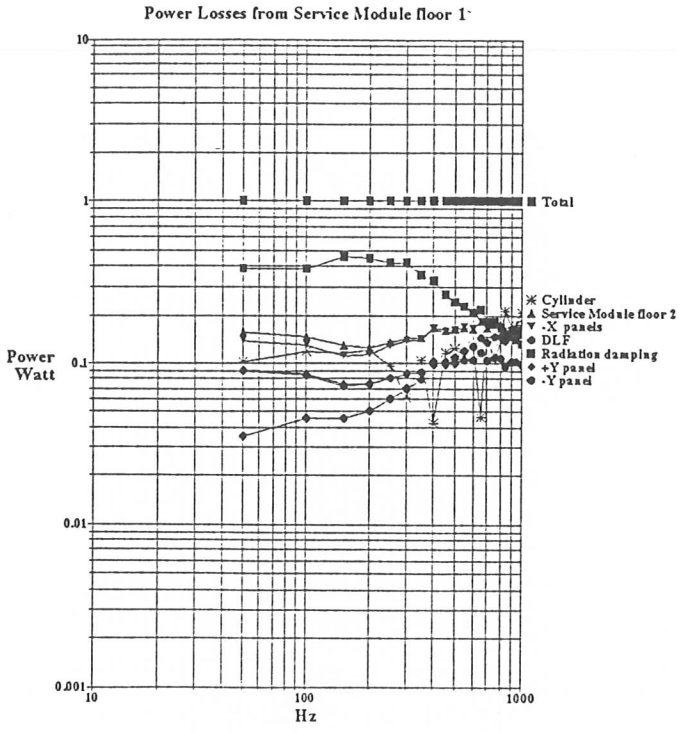

Figure 12. Power losses from SM floor 1

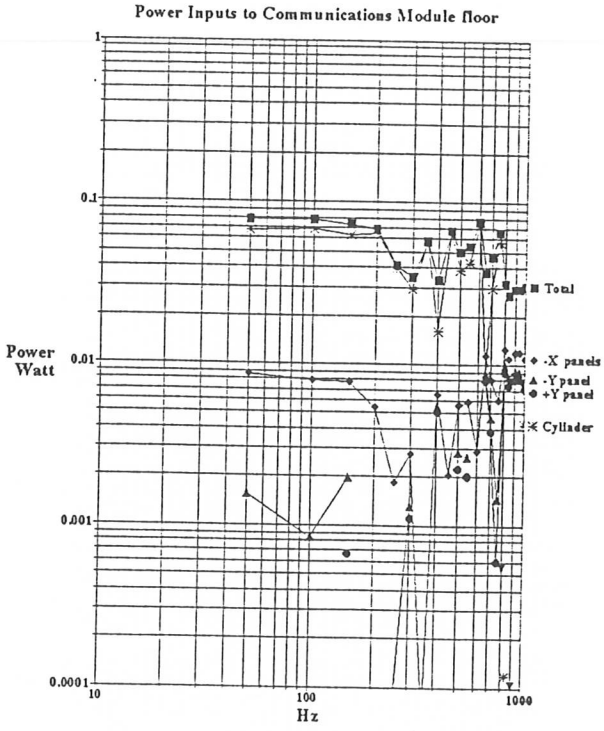

Figure 13. Power inputs to CM floor